TECHNICAL MEMORANDUMS

NATIONAL ADVISORY COMMITTEE FOR AERONAUTICS

No. 1059

AN EXPERIMENTAL INVESTIGATION OF THE FLOW OF AIR IN A FLAT BROADENING CHANNEL

By A. N. Vedernikoff

Central Aero-Hydrodynamical Institute

Washington
January 1944

NATIONAL ADVISORY COMMITTEE FOR AERONAUTICS

TECHNICAL MEMORANDUM NO. 1059

AN EXPERIMENTAL INVESTIGATION OF THE FLOW OF AIR IN A FLAT BROADENING CHANNEL*

By A. N. Vedernikoff

INTRODUCTION

The wide use of diffusers, in various fields of technology, has resulted in several experimental projects to study the action and design of diffusers. Most of the projects dealt with steam (steam turbine nozzles). But diffusers have other applications - that is, ventilators, smoke ducts, air coolers, refrigeration, drying, and so forth.

At present there is another application for diffusers in wind-tunnel design. Because of higher requirements and increased power of such installations more attention must be paid to the correctness of work and the decrease in losses due to every section of the tunnel.

A diffuser, being one of the component parts of a tunnel, can in the event of faulty construction introduce considerable losses. (See reference 1.) Therefore, in the design of the new CAHI wind tunnel, it was suggested that an experimental study of diffusers be made, with a view to applying the results to wind tunnels.

The experiments conducted by K. K. Baulin in the laboratories of CAHI upon models of diffusers (reference 2) of different cross sections, lengths, and angles of divergence, were a valuable source of experimental data. They were of no help, however, in reaching any conclusion regarding the optimum shape because of the complexity and diversity of the factors which all appeared simultaneously, thereby precluding the study of the effects of any one factor separately.

---

*Report No. 21[illegible], of the Central Aero-Hydrodynamical Institute, Moscow, 1926.

Note: Translation received from Massachusetts Institute of Technology, Cambridge, Mass.

On the suggestion of the director of the CAHI, Prof. B. N. Ureff, it was decided to experiment on a two-dimensional diffuser model and determine the effect of the angle of divergence. The author is acquainted with two experimental projects of like nature: the first was conducted with water (reference 3), the other with air (reference 4). The first of these works, although containing a wealth of experimental data, does not indicate the nature of flow or its relation to the angle of divergence. The second work is limited to four angles - that is, 12°, 24°, 45°, 90°. The study of this diffuser did not supply any information about the effect of smaller angles which, because of their advantages, are more commonly used. The author was able to acquaint himself with the second work only after the experiments were started. For these reasons, as well as because on the basis of those works no conclusion can be reached regarding the nature of flow distribution, of eddies, and so forth, experimental work was continued.

The need for determining flow patterns follows from the fact that from them are determined methods of measurement - that is, the determination of velocities by means of the pitot tube, which, as is well known, gives correct indications only when placed with its axis parallel to the axis of flow.

The data contained in this report were obtained from experiments conducted by the Aerodynamical Laboratories of the CAHI. The solutions to some of the mathematical problems connected with the experiments are due to Prof. S. A. Chapligin.

I

The model of a two-dimensional diffuser allowing a variation in the angle of 0° to 28° was constructed under the direction of Prof. B. N. Ureff. As shown in figure 1, the model has two movable walls the upper surfaces of which are covered with broadcloth, to form a better contact with a glass plate which forms the top of the diffuser. The entrance section of the diffuser had the following dimensions:

100 millimeters x 100 millimeters = 10^4 (mm^2) = 0.01 square meter.

The length of the diffuser was 10 times the entrance dimension

100 millimeters × 10 = 1.0 meter

The top plate was held in grooves as indicated in figure 1. The side walls were mounted on two spindles, which passed through two collars connected to the walls. With this arrangement it was possible to observe the flow by means of the usual wind vanes. The vanes were attached three to a holder with their axes 50 millimeters apart. The arrangement is indicated in figure 2(a). The lower plate of the diffuser was divided into 50-millimeter squares. Thus each vane could be placed at the centroid of the corresponding square.

For the determination of static pressures, the following method was used: Instead of a glass plate, a sheet of plywood was inserted in the grooves and taped down to avoid warping. Holes were drilled in this cover 50 millimeters apart along the axis, and 20 millimeters apart near the entrance section. Brass tubes 4 millimeters in diameter (fig. 2(c)) were inserted in the holes and connected by means of rubber tubing to a common collector (fig. 2(d)). Each rubber tube was equipped with a clip.

Connecting the manometer with the collector and removing any one of the clips made it possible to determine the static pressure at any point on the axis of the cover in the upper plane of the diffuser. Moving the cover in the grooves made possible measurement of the pressures along any line parallel to the axis of the diffuser. In view of the shallowness of the diffuser it was necessary to measure pressure only in one (upper) horizontal plane. A pitot tube was used to determine velocities (fig. 2(b)). A slit parallel to the axis was made down the length of the cover. A pitot tube was inserted in the slit which then was covered with Scotch tape (fig. 2(c)). By means of this arrangement it was possible to place the pitot tube at any point in the diffuser. The elevation of the tube was varied by means of a collar in which the tube was clamped. The pitot tube was first calibrated. The calibration curves are shown in figures 3 and 4.

The relation between h and v is expressed by

$$v \text{ meters per second} = \sqrt{\xi \frac{2gh}{\gamma}} \qquad (1)$$

where h is a millimeter of water, and the coefficient $\xi = 1$ (actually $\xi = 1.005$).

A battery manometer was used to determine static pressures. In determining the velocities by means of the pitot tube an R. Fuess No. 9814 manometer was used. The general view of the installation is shown in the photographs (figs. 5 and 6).

II

Flow spectrums for various angles of diffusion are shown in figures 7 to 13. Spectrums were taken every 2° from 0°. Thus the angles covered were 0°, 2°, 4°, 6°, 8°, 10°, 12°, 14°, 16°, 18°, 20°, 22°, 24°, and 26°.

The first seven spectrums, from 6° to 12°, did not deviate in any way from the usual flow pattern. The vanes were directed along lines leading to the apex of the diffuser and remained perfectly motionless. Fluctuation of the vanes was first observed at the end of the diffuser for an angle of 12°.

For $\alpha = 14^\circ$, the pattern was as shown in figure 7 - that is, at the end of the diffuser, near the right wall, a tendency for the vanes to rotate was apparent. This varied from a full revolution to a part of one. The arrows show the direction of rotation. Dotted arrows show that at that point the vane was vibrating. Some oscillations through a fixed angle are indicated by double dotted arrows.

A new phenomenon was observed for $\alpha = 16^\circ$. The region of vorticity increased in the direction of the entrance section; furthermore backflow appeared along one of the walls at the point marked with a double dotted arrow. The position of the vanes was unstable. The direction of rotation was unchanged - clockwise.

For $\alpha = 18^\circ$, new increase of the region of vorticity and increase of region of back flow along the wall are observed. Position of vanes is unstable along the left wall.

For $\alpha = 20^\circ$, vortices become more stable, but at some points the pattern varies with time. Fluctuation of vortices at a given point varies through a small angle. Region of vorticity and backflow is further increased.

For $\alpha = 22^\circ$, flow pattern remains generally unchanged, but becomes more complex with more intense vortices. A counterclockwise vortex appears along the left wall.

For $\alpha = 24^\circ$, region of unstable flow spreads throughout almost the whole diffuser. The extreme left vortex, at the right wall, becomes so intense at the high rotational speed that the vanes become invisible.

For $\alpha = 26^\circ$, vortices are displaced to the left side. Extreme left vortices are very close to the entrance section. Their intensity is so great that vanes are invisible. Backflow is observed along left wall. Direction of rotation of vortices is countercloskwise; flow unstable practically through the whole diffuser.

★ From the description it is easy to form a picture of the phenomenon. Apparently the flow changes at a certain angle - namely, 14° - followed by backflow along the walls and vortices. With increase of angle these phenomena increase both in intensity and region covered. The system of vortices may be near one wall at one instant and shift to the other wall a moment later. Hence the flow pattern is unstable. The experiment confirms theoretical deductions, since, according to the investigations of Prof. S. A. Chapligin for an ideal fluid, the vortex in a diffuser cannot be stable.

III

In figure 14 is shown a sketch of the diffuser.

Let

f_1 and f_2 = areas of sections 1 and 2

p_1 and p_2 = static pressures

v_1 and v_2 = velocities

γ_1 = density of air

γ_s = density of alcohols

p_o = atmospheric pressure

ξ = loss coefficient

Writing Bernoulli's equation for sections 1 and 2 yields

$$\frac{p_o}{\gamma} = \frac{p_1}{\gamma} + (1 + \xi_1)\frac{v_1^2}{2g} = \frac{p_2}{\gamma} + (1 + \xi_2)\frac{v_2^2}{2g} \quad (2)$$

Connecting the manometers to sections 1 and 2 and writing Bernoulli's equation gives

$$\frac{p_o}{\gamma} = \left(\frac{p_o}{\gamma} - h_1\frac{\gamma_s}{\gamma}\right) + \frac{v_1^2}{2g} \quad \text{(if small losses at entrance section are neglected)} \quad (3)$$

$$\frac{p_o}{\gamma} = \left(\frac{p_o}{\gamma} - h_2\frac{\gamma_s}{\gamma}\right) + (1 + \xi_2)\frac{v_2^2}{2g} \quad (4)$$

Let X be the "quality" of the diffuser.

$$X = \frac{v_1^2}{2g} : (1 + \xi_2)\frac{v_2^2}{2g} \quad (5)$$

Substituting in equation (5) for

$$\frac{v_1^2}{2g} \quad \text{and} \quad (1 + \xi_2)\frac{v_2^2}{2g}$$

yields, from equations (3) and (4),

$$X = \frac{h_1\frac{\gamma_s}{\gamma}}{h_2\frac{\gamma_s}{\gamma}} = \frac{h_1}{h_2} \quad (6)$$

Thus, the quality is expressed by the ratio of the heights of the columns of alcohol at sections 1 and 2.

Measuring h_1 and h_2 for different angles of diffusion and taking the ratio $(h_1 : h_2)$ yields quality as a function of the angle. Owing to the fact that the transverse pressure distribution at section 1 is nonuniform, the battery manometer was connected there at three points. The quality was found from

$$X = \frac{h_1' + h_1'' + h_1'''}{3} : h_2 \qquad (7)$$

where h_1', h_1'', h_1''', are the measured heads at section 1; and h_2 is the measured head at section 2.

The quality was determined for two different entrance velocities. The curve of quality against angle is given in figure 15. The dotted line represents the curve obtained at the second speed. The maximum quality $X = 4.13$ occurs at $\alpha = 14^\circ$. For the rising part of the curve, the change in speed becomes apparent from 10°. For angles less than 10° the two curves coincide.

IV

The investigation of the dynamic pressure distributions throughout the diffuser was of considerable interest. In figures 16 to 22 are shown dynamic pressure distributions in millimeters of water, down the length of the diffuser for various angles.

For $\alpha = 0^\circ$, q increases along the diffuser axis (static pressure decreases) (fig. 16). From figures 17 to 22 it follows that maximum q does not coincide with the entrance of the diffuser but is displaced downstream. This is due to the contraction of the stream at the entrance. The curves appear to be smooth for angles up to 12°. From 16° the curves become somewhat irregular, which indicates unstable flow. In figure 23 is shown a curve of (h/h_0) where h_0 is the dynamic pressure head at the end section and h is the average dynamic pressure head. In figure 24 this is represented on a three-dimensional system of coordinates.

The isobars along the diffuser are shown in figures 25 to 30. The isobars (lines of constant pressure) are plotted nondimensionally - that is, relative to the end section q.

From the plots it is evident that the most uniform isobar distribution is obtained for 8° and 12°. With an increase in the angle, the isobars "tighten" up in the direction of the entrance section and their magnitude decreases. All this points to the fact that, for large angles of diffusion, there occurs a decrease in output, a decrease in the created pressure gradient, and an extremely inefficient utilization of the end section. This is confirmed by the flow spectrums as well as the curve of figure 15.

V

The velocities were measured by means of a pitot tube the calibration curve for which is shown in figures 3 and 4. For the determination of velocity distributions in the entrance section measurements were made at 25 points, as shown in figure 31.

Velocities were determined for $\alpha = 0^\circ$ and $\alpha = 24^\circ$, varying the speed by 1 meter per second. Experiments were made at four different speeds. The velocity distribution for $\alpha = 0^\circ$ is shown in figures 32 to 35. Evidently the pattern remains stable for all four speeds. The velocity distribution for $\alpha = 24^\circ$ is shown in figures 36 to 39. It is seen here that the distribution across the section is unstable. Hence, an increase in the angle of diffusion tends to distort the velocity distribution at the entrance section. This effect becomes more pronounced as the angle is increased.

The velocity distribution in the horizontal plane which bisects the diffuser is given in figures 40 to 43. For angles greater than 12°, the velocities were not measured, owing to the appearance of vortices and backflow. The velocity of backflow was negligible compared to the direct velocity. The direction of backflow varied rapidly and the attempt to determine the instantaneous velocity and direction was a difficult task. The method of twin tubes, usually applicable to such problems, does not give reliable results in the present case; therefore it was decided not to make those measurements.

In figure 43 it is noticeable that the velocity along the left wall, at the end section, approaches zero, which implies the possible appearance of backflow along this wall.

VI

Since the reciprocal of quality $1/X$ gives the sum of all the losses as a function of α, the curve of $1/X$ was used to determine the relation between the different losses and the angle α.

Friction losses were computed from:

$$\Delta T = k_f \Delta F \, v^3 \tag{8}$$

where

k_f = coefficient of friction = 0.0002

ΔF = element of diffuser surface

v = velocity

$$h_o = h_1$$

In our case (fig. 44)

$$h_o = b_o$$

$$k = \tan \frac{\alpha}{2}$$

$$b = b_o + 2kx$$

$$b_1 = b_o + 2kl$$

$$s = 2(b + h_o)$$

$$\Delta F = 2 (b + h_o) \Delta x = 2 (b_o + 2kx + h_o) \Delta x$$

$$= \left[2 (b_o + h_o) + 4kx\right] \Delta x \tag{9}$$

$$\Delta T = k_f \Delta F v^3 = k_f \Delta F v_o^3 \left(\frac{b_o}{b_o + 2kx}\right)^3$$

$$= \frac{2(b_o + 2kx + h_o)\Delta x v_o^3 b_o^3}{(b_o + 2kx)^3} k_f$$

$$= \frac{4(h_o + kx)}{(h_o + 2kx)^3} \Delta x v_o^3 h_o^3 k_f$$

$$= \frac{A}{B} \Delta x v_o^3 h_o^3 k_f \qquad (10)$$

The kinetic energy at the entrance section is

$$T_o = \frac{m v_o^2}{2} = \frac{b_o h_o v_o \gamma}{2g} v_o^2 = \frac{h_o^2 v_o^3}{16} \qquad (11)$$

Friction loss along total length of diffuser is T_f

Let

$$\frac{A}{B} = f(x) \qquad \text{(See equation (10).)}$$

then

$$T_f = \int_o^x f(x)\, dx\, v_o^3 h_o^3 k_f \qquad (12)$$

To evaluate the integral, $f(x)$ is plotted for different values of α. (See fig. 45.)

By integration of $f(x)$ graphically between 0 and x a graph of

$$\int_o^x f(x)\, dx$$

is obtained.

Let ξ be the ratio of work lost in friction to the total kinetic energy at the entrance section.

$$\xi = \frac{T_f}{T_o} = \frac{v_o^3 h_o^3 k_f \, 16}{b_o \, h_o \, v_o^3} \int_o^x f(x) \, dx$$

that is,

$$\xi = C \int_o^x f(x) \, dx \tag{13}$$

where

$$C = b_o \, k_f \, 16$$ (See fig. 46.)

The ratio of the kinetic energy at any section to the entrance section kinetic energy is W_2/W_1. (See fig. 46.)

$$\frac{W_2}{W_1} = \frac{h_o \, (b_o + 2kl) \, v_1^3 \gamma}{2g} : \frac{b_o \, h_o \, v_o^3 \gamma}{2g}$$

$$= \frac{h_o \, (b_o + 2kl) \, v_o^3 \, b_o^3}{(b_o + 2kl)^3 \, b_o \, h_o \, v_o^3} \quad \frac{b_o^2}{(b_o + 2kl)^2} \tag{14}$$

The graph of $1/X$ is given in figure 48.

After the ordinates of ξ and W_2/W_1 are subtracted from the ordinate of $1/X$, the remaining ordinates give the hydraulic losses. The curve of hydraulic losses is shown in figure 49. From this it may be seen that the minimum hydraulic loss occurs at $\alpha = 8^\circ$.

CONCLUSION

On the basis of the results obtained, the nature of the operation of the diffuser can be deduced.

The flow remains stable only between $\alpha = 0^\circ$ and $\alpha = 14^\circ$. Beginning with $\alpha = 14^\circ$, the flow becomes unstable; vortices are formed. The axes of the vortices arrange themselves first along one wall, then along the other. With increase of angle, the vortices become more numerous and more intense. The more intense vortices occur near the entrance section. Backflow appears along the walls.

The quality of a diffuser is a function of the angle of diffusion and increases as the angle. At a certain angle α, this increase stops abruptly and vortices start forming. This coincidence between the magnitude of the quality and the nature of flow was clearly brought out by the experiments.

Maximum quality (4.13) occurred at $\alpha = 14^\circ$. From the calculated losses, it was found that minimum hydraulic loss occurred at $\alpha = 8^\circ$ to 10°. This is confirmed by the isobar patterns.

Translation by G. S. Cherniak.

REFERENCES

1. Ushakov, K. A.: Wind-Tunnels and Their Properties. USSR Air Corps Bull. No. 4, 1923.

2. Baulin, K.: Experimental Study on Air Channels. Trans. CAHI No. 7 (USSR).

3. Hochschild, H.: Versuche über die Strömungsvergänge in erweiterten und verengten Kanälen. Forschungsarbeiten auf dem Gebiete des Ingenieurwesens, No. 114.

4. Kröner, R.: Versuche über Strömungen in stark erweiterten Kanälen. Forschungsarbeiten auf dem Gebiete des Ingenieurwesens, No. 222.

Table I. - Calibration of pitot tube.

h mm	25	35	45	55	70	80	90	100	115	125	130	140	165
vm/sec	13.0	15.0	17.5	19.0	21.5	23.0	24.0	25.5	27.0	28.5	29.0	30.0	32.5
$h_w=0,4hs$	10	14	18	22	28	32	36	40	46	50	52	56	66

Table II.- Determination of X.

	0°	2°	4°	6°	8°	10°	12°	14°	16°	18°	20°	22°	24°	26°	28°
h'_1	18	28	40	54	68	78	86	90	80	75	66	55	45	45	42
h''_1	16	25	36	48	60	69	76	80	70	67	60	50	38	38	34
h'''_1	18	28	40	54	68	78	86	90	80	75	66	55	45	45	40
h_2	21	22	21	21	21	21	21	21	21	23	23	22	22	24	24
X	0.825	1.23	1.85	2.48	3.10	3.57	3.94	4.13	3.65	3.14	2.78	2.42	1.94	1.78	1.61
h'_1	22	35	50	68	84	98	104	116	104	90	72	64	60	55	49
h''_1	20	31	45	60	74	85	90	100	90	80	60	54	50	45	40
h'''_1	22	35	50	67	84	98	104	116	104	90	66	58	52	48	42
h_2	26	27	26	26	26	26	26	28	28	28	28	28	28	27	29
X	0.82	1.25	1.86	2.5	3.10	3.60	3.82	3.96	3.55	3.10	2.36	2.10	1.93	1.83	1.50

Table III.- Negative pressure h along axis in mm of water. 0°.

	1	2	3	4	5	6
a	15	18	21	23	26	27
c	16	19	22	25	27	29
e	16	19	22	25	28	30
1	16.2	19.5	23	26	28	30
2	16.2	20	23	26	28	30
3	16.2	20	23	26	28	30
5	17	20	24	26	29	31
8	17	21	24	27	30	32
11	18	22	25	29	31	33
15	19	23	26	30	33	35
Chamber	21	26	30	33	36	39

Table IV.- Negative pressure h along axis in mm of water. 4°.

	1	2	3	4	5	6
a	34	40	48	52	56	62
c	36	42	50	54	60	65
e	35	42	48	54	59	64
1	34	40	47	52	58	63
2	33	39	46	50	56	60
3	32	38	43	48	53	58
5	29	35	40	44	50	53
8	26	32	36	40	44	48
11	24	30	34	37	41	45
15	22	27	31	34	37	40
Chamber	22	26	30	33	36	39

Table V.- Negative pressure h along axis in mm of water. 8°.

	1	2	3	4	5	6
a	51	63	72	80	90	98
c	53	65	76	85	94	103
e	51	62	73	80	90	97
1	47	58	67	75	82	90
2	43	52	62	68	75	82
3	40	48	57	62	70	75
5	35	42	50	54	60	66
8	30	36	42	46	50	55
11	26	32	36	40	45	49
15	23	27	32	35	39	42
Chamber	22	26	30	33	36	40

Table VI.- Negative pressure h along axis in mm of water. 12°.

	1	2	3	4	5	6
a	57	70	80	89	98	108
c	61	75	85	93	104	116
e	58	73	82	90	102	112
1	54	69	74	84	90	102
2	48	60	66	74	81	88
3	45	53	60	66	70	80
5	37	45	50	56	60	67
8	30	36	40	45	49	55
11	26	32	35	40	44	50
15	23	28	31	34	38	42
Chamber	21	26	28	32	36	39

Table VII. Negative pressure h along axis in mm of water. 16°.

	1	2	3	4	5	6
a	48	59	71	80	82	90
c	52	64	73	85	90	95
e	53	62	70	83	89	95
1	48	62	66	78	86	86
2	44	57	62	67	78	82
3	40	50	56	62	69	70
5	32	41	48	50	54	60
8	27	34	37	41	45	48
11	24	30	35	36	41	43
15	22	27	31	34	37	40
Chamber	21	26	30	32	36	38

Table VIII. Negative pressure h along axis in mm of water. 20°.

	1	2	3	4	5	6
a	42	52	58	64	70	70
c	46	55	60	71	72	72
e	45	52	60	68	69	70
1	44	48	58	66	68	68
2	41	48	53	61	62	62
3	36	43	47	55	57	56
5	30	36	40	45	47	50
8	25	31	35	38	41	44
11	24	28	32	35	38	42
15	22	27	31	33	36	40
Chamber	21	26	30	32	34	38

Table IX. Negative pressure h along axis in mm of water. 24°.

	1	2	3	4	5	6
a	38	43	50	54	63	60
c	39	46	53	56	65	63
e	37	45	52	55	63	63
1	36	44	50	52	61	61
2	35	41	46	49	55	58
3	32	35	42	45	54	54
5	27	30	36	39	45	46
8	23	28	33	36	41	42
11	23	27	31	34	38	40
15	22	26	31	34	37	39
Chamber	21	26	30	33	36	38

Table X. Ratio of mean pressure along axis to pressure in chamber. $h_m : h$

	0°	4°	8°	12°	16°	20°	24°
a	0.701	1.57	2.42	2.76	2.35	1.97	1.68
c	0.745	1.65	2.54	2.94	2.50	2.10	1.76
e	0.755	1.62	2.42	2.84	2.47	2.02	1.72
1	0.770	1.58	2.24	2.60	2.32	1.95	1.66
2	0.770	1.52	2.04	2.30	2.13	1.82	1.55
3	0.770	1.45	1.88	2.06	1.90	1.64	1.42
5	0.795	1.35	1.64	1.74	1.56	1.37	1.21
8	0.831	1.21	1.38	1.40	1.27	1.18	1.10
11	0.855	1.13	1.22	1.24	1.14	1.10	1.05
15	0.898	1.03	1.06	1.08	1.04	1.04	1.03
Chamber	1.0	1.0	1.0	1.0	1.0	1.0	1.0

Table XI.- Pressure in mm of water. $\alpha = 8^{\circ}$.

	0	a	b	c	d	e	1	2	3	4	5	6	7	8	9	10	11	12	13	14	15	16	17
−90	—	—	—	—	—	—	—	—	—	—	—	—	—	—	—	—	24	22	21	22	20	20	19
−80	—	—	—	—	—	—	—	—	—	—	—	—	—	26	25	24	—	—	—	—	—	—	—
−70	—	—	—	—	—	—	—	—	—	—	31	29	28	26	25	25	24	22	21	21	21	20	19
−60	—	—	—	—	—	—	—	35	34	34	31	29	28	25	25	25	—	—	—	—	—	—	—
−50	57	55	50	47	45	41	40	35	34	33	31	29	28	25	25	25	24	23	21	21	21	20	20
−40	54	54	49	46	44	41	40	35	34	33	31	29	28	—	—	—	—	—	—	—	—	—	—
−30	47	49	47	45	44	42	40	34	35	33	31	29	28	27	25	24	24	22	21	21	21	20	20
−20	45	45	47	45	44	41	39	34	34	32	31	29	27	—	—	—	—	—	—	—	—	—	—
−10	43	46	44	45	43	41	39	35	34	33	31	20	28	—	—	—	—	—	—	—	—	—	—
0	44	44	45	43	43	40	40	35	33	32	31	29	27	25	25	25	23	22	21	21	21	20	20
+10	43	45	43	44	43	40	40	37	34	32	30	29	27	—	—	—	—	—	—	—	—	—	—
+20	46	45	43	44	43	40	40	37	34	31	30	28	28	—	—	—	—	—	—	—	—	—	—
+30	47	47	45	43	42	43	40	36	35	32	30	20	27	26	25	24	24	22	21	21	21	20	20
+40	53	49	45	42	43	43	39	37	35	31	31	28	27	—	—	—	—	—	—	—	—	—	—
+50	57	52	46	42	41	41	39	37	34	31	31	29	27	25	25	25	24	22	21	21	21	21	20
+60	—	—	—	—	—	—	—	37	34	32	31	29	26	25	25	25	—	—	—	—	—	—	—
+70	—	—	—	—	—	—	—	—	—	—	30	29	26	25	25	25	23	22	21	21	21	20	20
+80	—	—	—	—	—	—	—	—	—	—	—	—	—	25	26	25	—	—	—	—	—	—	—
+90	—	—	—	—	—	—	—	—	—	—	—	—	—	—	—	—	21	22	21	21	21	20	19

Table XII.- $\alpha = 12^{\circ}$.

	0	a	b	c	d	e	1	2	3	4	5	6	7	8	9	10	11	12	13	14	15	16	17
−110	—	—	—	—	—	—	—	—	—	—	—	—	—	—	—	23	22	22	21	21	20	20	20
— 90	—	—	—	—	—	—	—	—	—	—	—	28	27	26	24	23	23	23	22	21	21	21	20
— 70	—	—	—	—	—	—	—	—	31	30	28	26	25	23	22	23	22	21	21	20	20	20	20
— 60	—	—	—	—	—	42	40	36	34	31	30	27	26	25	25	23	22	23	22	22	21	21	20
— 50	48	46	46	43	42	42	39	37	32	31	29	28	26	25	24	24	23	23	22	23	22	21	21
— 40	45	48	44	44	46	44	43	38	34	32	29	28	26	25	24	24	23	22	21	21	21	21	20
— 20	47	50	48	50	50	47	46	42	38	35	31	30	26	26	25	24	23	23	23	22	22	21	21
0	43	43	44	43	45	42	41	40	34	32	30	29	27	26	27	25	24	24	24	24	23	22	21
+ 20	43	44	46	45	43	41	40	38	34	34	30	29	29	28	26	25	25	24	23	23	22	22	22
+ 40	45	45	41	40	38	36	36	33	32	31	29	28	25	25	24	23	23	22	22	22	21	21	21
+ 50	50	52	49	43	41	40	40	35	33	30	28	27	27	27	24	24	24	22	22	22	22	21	21
+ 60	—	—	—	—	—	40	38	35	32	31	30	27	26	26	25	24	24	23	23	22	22	22	21
+ 70	—	—	—	—	—	—	—	—	35	32	30	29	26	27	25	24	24	24	23	23	22	21	21
+ 90	—	—	—	—	—	—	—	—	—	—	—	28	28	25	25	25	23	23	23	22	22	22	21
+110	—			—	—	—	—	—	—	—	—	—	—		—	24	23	23	23	22	22	22	21

Table XIII.- $\alpha = 16^{\circ}$.

	0	a	b	c	d	e	1	2	3	4	5	6	7	8	9	10	11	12	13	14	15	16	17
— 130	—	—	—	—	—	—	—	—	—	—	—	—	—	—	—	—	23	23	23	23	22	22	21
— 110	—	—	—	—	—	—	—	—	—	—	—	—	—	25	24	24	23	22	22	21	21	21	21
— 90	—	—	—	—	—	—	—	—	—	—	28	26	25	24	24	23	23	22	22	21	21	21	21
— 70	—	—	—	—	—	—	—	36	32	30	27	27	25	24	23	23	22	22	21	21	21	21	21
— 60	—	—	—	—	40	36	36	33	30	27	26	25	25	23	23	23	22	22	21	21	21	21	21
— 50	46	46	44	44	42	40	39	35	32	26	26	25	24	24	23	22	22	21	21	22	22	22	22
— 40	40	40	41	38	40	38	37	35	29	28	25	25	24	23	21	21	21	21	21	21	21	21	21
— 20	34	34	33	36	37	34	34	30	30	27	25	24	23	23	22	22	22	21	21	21	21	21	21
0	32	37	37	35	35	34	33	32	28	30	27	25	25	24	23	23	23	22	22	22	21	21	21
+ 20	36	35	35	33	35	35	32	33	31	28	26	26	25	24	23	23	22	22	21	21	21	21	21
+ 40	42	43	38	35	34	32	32	31	31	29	27	25	24	23	23	22	22	22	21	21	21	21	21
+ 50	48	48	44	42	42	36	35	35	32	30	28	26	25	25	23	23	23	22	22	21	21	21	21
+ 60	—	—	—	—	40	36	33	32	29	30	27	26	25	25	23	23	23	22	22	21	21	21	21
+ 70	—	—	—	—	—	—	—	30	31	28	26	25	24	24	23	22	21	21	21	21	21	21	21
+ 90	—	—	—	—	—	—	—	—	—	—	27	26	25	24	23	23	22	22	22	22	21	21	21
+ 110	—	—	—	—	—	—	—	—	—	—	—	—	—	24	24	24	23	22	22	21	22	22	21
+ 130	—	—	—	—	—	—	—	—	—	—	—	—	—	—	—	—	23	22	22	22	22	22	21

Table XIV.- $\alpha = 20^{\circ}$.

	0	a	b	c	d	e	1	2	3	4	5	6	7	8	9	10	11	12	13	14	15	16	17
-150	—	—	—	—	—	—	—	—	—	—	—	—	—	—	—	20	20	—	19	—	19	—	19
-130	—	—	—	—	-	—	—	—	—	—	—	—	—	20	20	20	20	—	19	—	19	—	19
-110	—	—	—	—	—	—	—	—	—	—	—	22	22	21	21	20	20	—	19	—	19	—	19
- 90	—	—	—	—	—	—	—	—	26	24	23	23	21	21	21	20	20	—	19	—	19	—	19
- 70	—	—	—	—	—	—	25	27	26	26	23	23	21	21	21	20	20	—	19	—	19	—	19
- 60	—	—	—	32	32	32	30	28	25	24	23	22	21	20	20	20	19	—	19	—	19	—	19
- 50	36	33	33	34	33	32	31	28	24	24	23	22	21	21	21	21	20	—	19	—	19	—	19
- 40	32	32	31	32	32	31	31	28	26	24	24	22	22	21	20	21	20	—	19	—	19	—	19
- 20	30	31	31	31	31	29	30	30	25	24	22	21	21	20	20	20	20	—	19	—	19	—	19
0	29	28	30	28	29	29	30	28	27	25	23	22	22	21	20	20	19	—	19	—	19	—	19
+ 20	29	30	30	31	31	28	29	28	27	25	23	22	21	20	20	20	20	—	19	—	19	—	19
+ 40	40	37	35	33	32	30	30	28	27	26	24	24	23	22	22	20	20	—	19	—	19	—	19
+ 50	40	40	36	34	30	30	28	27	26	23	23	22	22	21	20	20	20	—	19	—	19	—	19
+ 60	—	—	—	34	32	32	27	26	25	24	23	22	22	22	22	21	20	—	19	—	19	—	19
+ 70	—	—	—	—	—	—	28	27	25	25	23	23	22	21	21	20	20	—	20	—	20	—	19
+ 90	—	—	—	—	—	—	—	—	26	24	24	23	21	21	20	20	20	—	19	—	19	—	19
+110	—	—	—	—	—	—	—	—	—	—	—	22	21	20	20	20	20	—	20	—	19	—	19
+130	—	—	—	—	—	—	—	—	—	—	—	—	—	21	21	20	20	—	20	—	20	—	19
+150	—	—	—	—	—	—	—	—	—	—	—	—	—	—	—	20	20	—	20	—	20	—	20

Table XV.- $\alpha = 24^\circ$.

	0	a	b	c	d	e	1	2	3	4	5	6	7	8	9	10	11	12	13	14	15	16	17
−140	—	—	--	—	—	—	—	--	—	--	---	—	—	19	19	19	—	—	19	—	19	—	19
−120	—	—	--	—	—	—	—	—	—	—	—	20	20	19	19	19	—	—	19	—	19	—	19
−100	—	—	—	-	--	—	—	—	—	21	21	20	20	20	20	19	—	—	19	—	19	—	19
− 80	—	—	—	—	—	—	—	27	25	23	22	22	22	21	21	21	—	—	20	—	20	—	20
− 70	—	—	—	—	—	34	32	29	26	23	22	21	21	20	20	19	—	—	19	—	19	—	19
− 60	—	—	—	32	30	29	28	26	24	22	21	20	20	20	20	20	—	—	19	—	19	—	19
− 50	33	33	34	32	32	32	32	28	26	24	23	22	20	20	20	19	—	—	19	—	19	—	19
− 40	32	31	30	30	31	32	31	26	23	23	22	22	21	20	20	20	—	—	19	—	19	—	19
− 20	28	29	30	30	30	29	30	27	24	22	21	21	20	20	20	19	—	—	19	—	19	—	19
0	30	30	31	32	31	30	29	30	25	24	23	22	21	21	21	20	—	—	20	—	19	—	19
+ 20	33	33	34	30	30	30	28	27	26	24	23	22	22	21	20	20	—	—	20	—	20	—	20
+ 40	40	35	34	33	30	27	27	25	25	24	23	22	22	21	20	20	—	—	19	—	19	—	19
+ 50	42	40	38	35	32	30	30	27	25	24	22	22	21	20	21	19	—	—	19	—	19	—	19
+ 60	—	—	—	36	31	31	27	27	25	24	23	21	20	21	20	20	—	—	19	—	19	—	19
+ 70	—	—	—	—	—	27	29	26	24	23	22	21	21	20	20	20	—	—	19	—	19	—	19
+ 80	—	—	—	—	—	—	—	25	25	24	22	20	21	20	20	19	—	—	19	—	19	—	19
+100	—	—	—	—	—	—	—	—	—	23	21	20	20	20	19	20	—	—	19	—	19	—	19
+120	—	—	—	-	—	—	—	—	—	—	—	20	20	19	19	19	—	—	19	—	19	—	19
+140	—	—	—	—	—	—	—	—	—	—	—	—	—	19	19	19	—	—	19	—	19	—	19

Table XVI.- Velocities in initial section. $\alpha = 0^{\circ}$.

	Сеч.	−4	−2	0	+2	+4
1 terminal	1	33	30	30	30	33
	2	31	30	30	30	30
	3	35	32	31	33	36
	4	37	33	32	32	36
	5	37	35	34	35	38
2 terminal	1	40	36	35	37	40
	2	38	37	37	37	40
	3	42	40	39	40	44
	4	44	40	38	40	44
	5	46	43	43	43	48
3 terminal	1	43	42	42	43	47
	2	45	45	45	46	46
	3	50	46	45	47	53
	4	52	46	45	46	52
	5	55	51	50	52	56
4 terminal	1	45	45	44	44	46
	2	50	50	49	49	51
	3	55	51	51	52	60
	4	60	53	51	53	60
	5	60	56	56	57	60

Table XVII.- Velocities in initial section. $\alpha = 24^{\circ}$.

	Сеч.	−4	−2	0	+2	+4
1 terminal	1	65	75	75	80	85
	2	80	85	85	95	80
	3	70	85	85	85	70
	4	75	100	85	95	75
	5	70	90	85	80	75
2 terminal	1	90	85	85	95	80
	2	105	100	105	110	95
	3	85	95	100	85	85
	4	90	110	100	125	90
	5	90	115	110	130	85
3 terminal	1	115	95	90	90	95
	2	110	110	120	120	115
	3	100	110	110	110	100
	4	105	120	105	110	110
	5	100	140	130	120	100
4 terminal	1	120	115	110	120	110
	2	130	130	130	140	135
	3	110	115	110	110	115
	4	120	140	140	145	115
	5	105	130	125	130	110

Manometer readings multiplied by factor 0.4, velocities determined by formula (1).

Table XVIII.- Velocities in center plane of diffuser.

Сеч.	$\alpha = 0°$					$\alpha = 4°$					$\alpha = 8°$					$\alpha = 12°$				
	−4	−2	0	+2	+4	−4	−2	0	+2	+4	−4	−2	0	+2	+4	−4	−2	0	+2	+4
0	32	30	30	30.5	33	46	44	44	45	49	90	95	96	99	95	76	94	98	98	82
	14.6	14.2	14.2	14.3	14.8	17.5	17.3	17.3	17.4	18.2	24.0	24.8	25.0	25.4	24.8	22.4	24.7	25.3	25.3	23.0
1	31	33	33	33	32	48	48	48	49	48	74	79	82	80	72	76	82	80	80	76
	14.4	14.8	14.8	14.8	14.6	18.0	18.0	18.0	18.2	18.0	22.0	22.7	23.0	22.8	21.7	22.4	23.0	22.8	22.8	22.4
5	31	33	34	34	32	33	35	37	39	40	61	63	64	63	61	57	57	57	56	56
	14.4	14.8	15	15	15.6	14.8	15.2	15.8	16.0	16.3	20	20.3	20.5	20.3	20	19.5	19.5	19.5	19.3	19.3
9	32	35	35	34	32	35	36	34	34	32	50	51	51	51	51	44	44	47	45	44
	14.6	15.2	15.2	15.0	14.6	15.2	15.6	15.0	15.0	14.6	18.2	18.4	18.4	18.4	18.4	17.3	17.3	17.8	17.4	17.3
13	25	33	33	33	25	32	32	31	32	32	43	46	42	45	45	34	36	35	33	38
	13.0	14.8	14.8	14.8	13.0	14.6	14.6	14.4	14.6	14.6	17.0	17.5	16.8	17.4	17.4	15.0	15.6	15.2	14.8	16.0
17	31	31	32	32	30	38	38	35	38	38	40	37	39	38	45	25	27	30	25	28
	14.4	14.4	14.6	14.6	14.2	16.0	16.0	15.2	16.0	16.0	16.3	15.8	16.0	15.9	17.4	13.0	13.4	14.2	13.0	13.6

Примечание. Вторые строки таблицы (m/sec) подсчитаны согласно примечаний к табл. XVI и XVII.

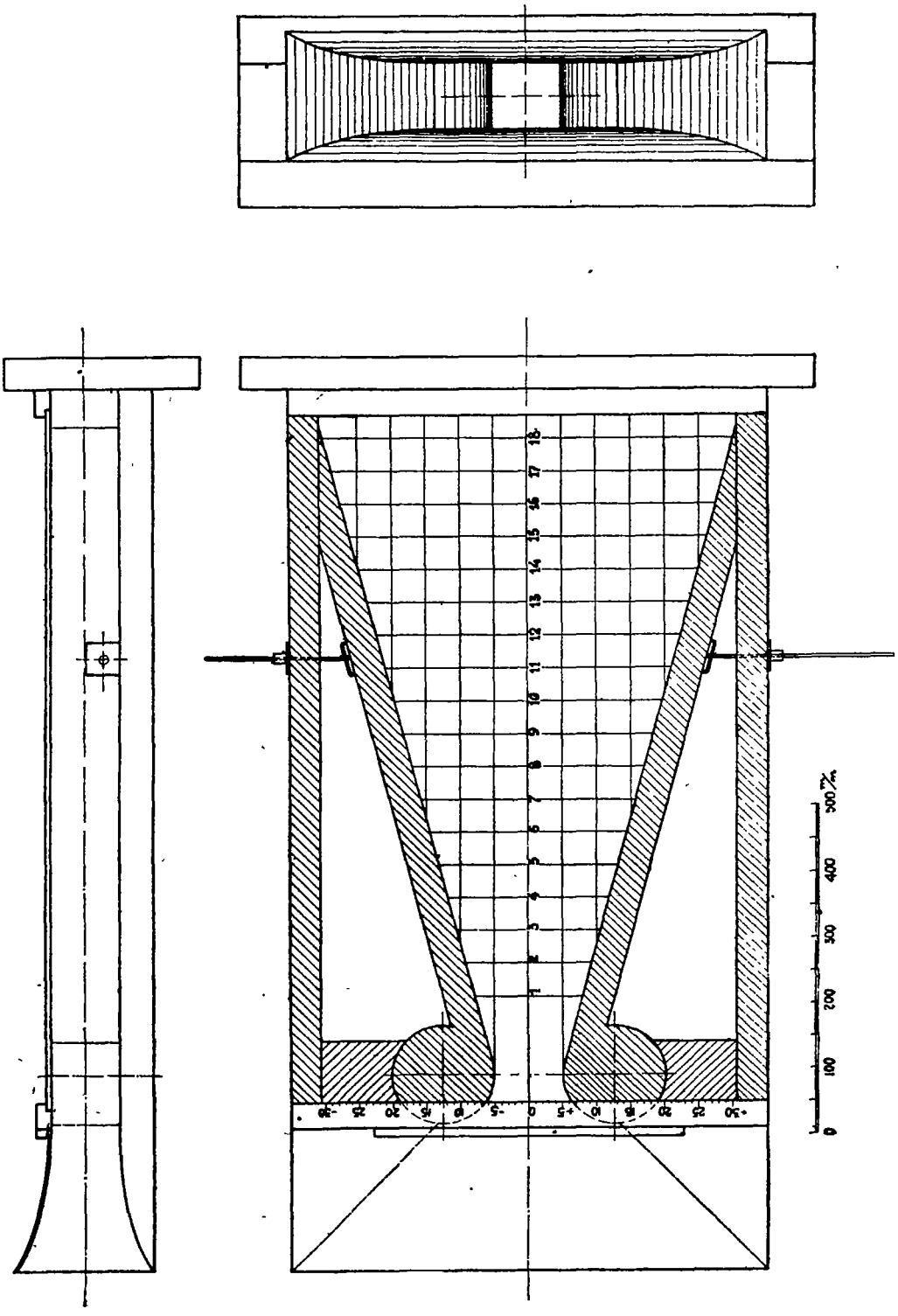

Figure 1.

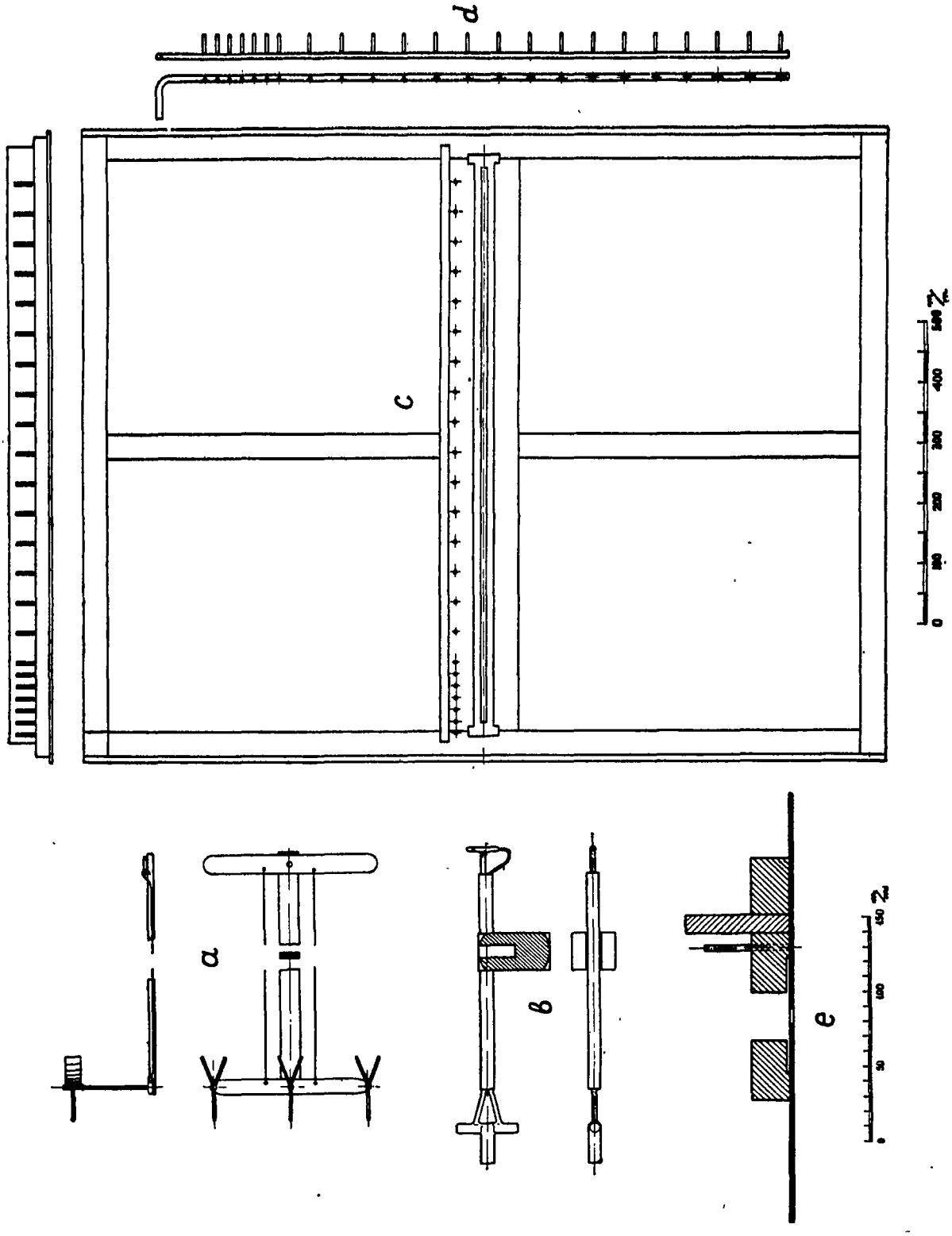

Figure 2.

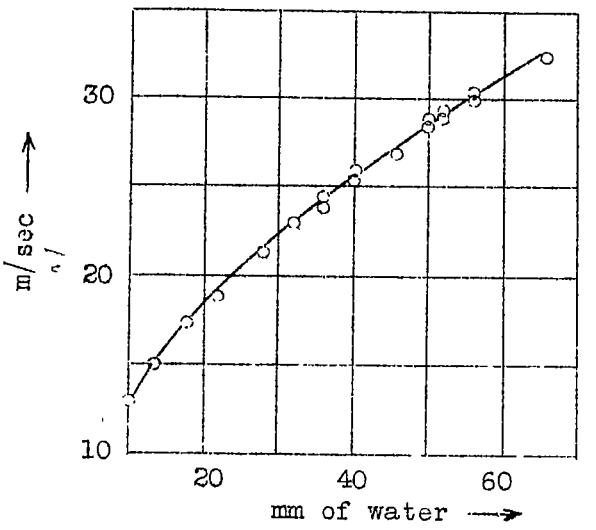
30
20
10
m/sec
20
40
60
mm of water

Fig. 3.

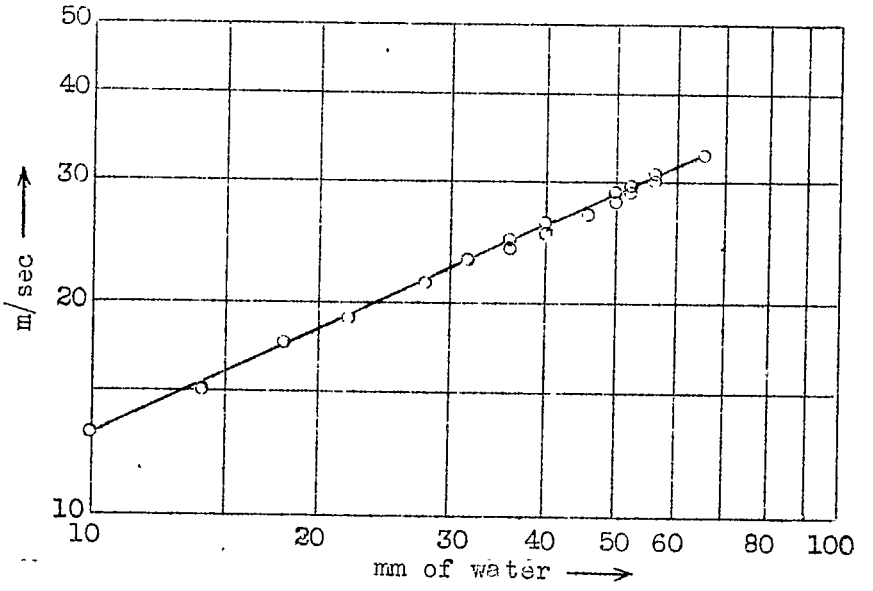
50
40
30
20
10
m/sec
10
20
30
40
50
60
80
100
mm of water

Fig. 4.

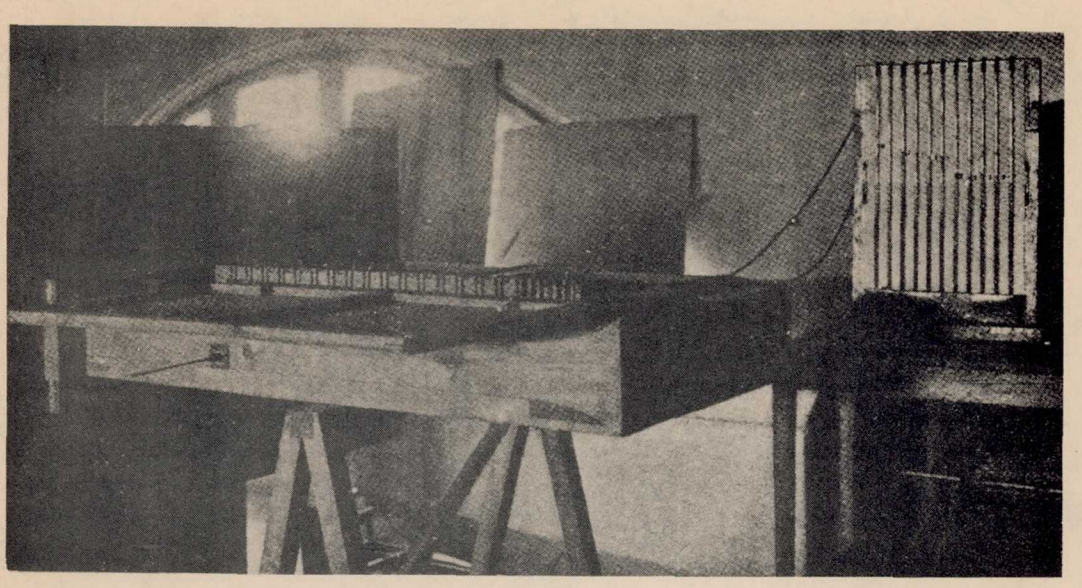

Figure 5.

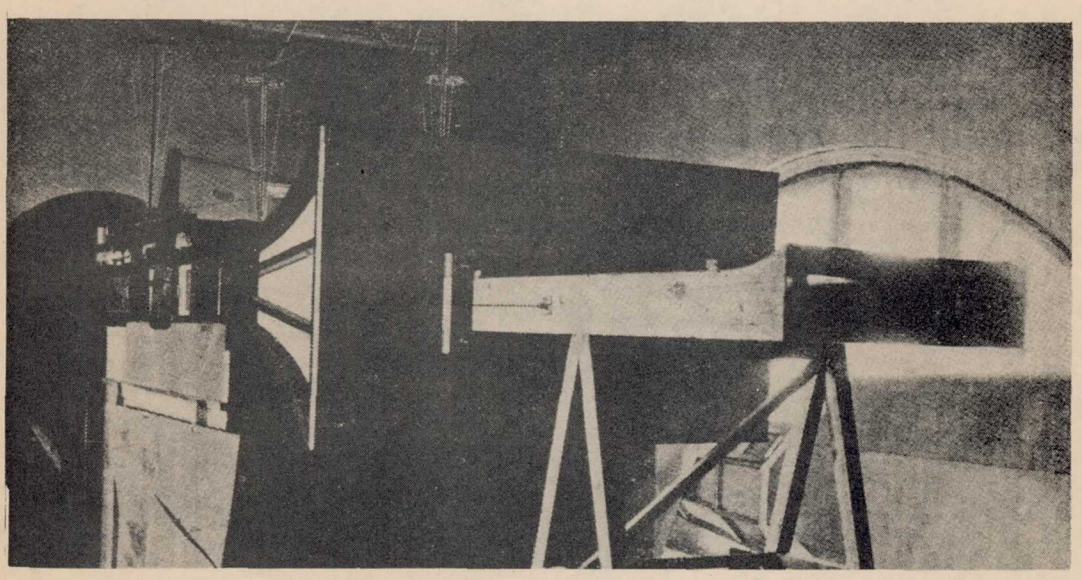

Figure 6.

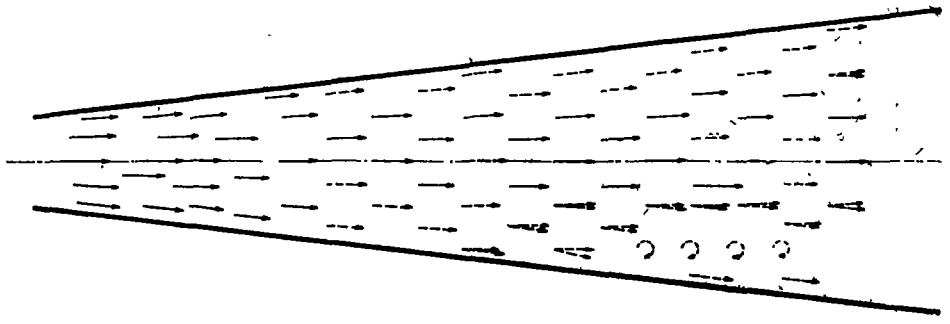

Figure 7. $\alpha = 14^{\circ}$.

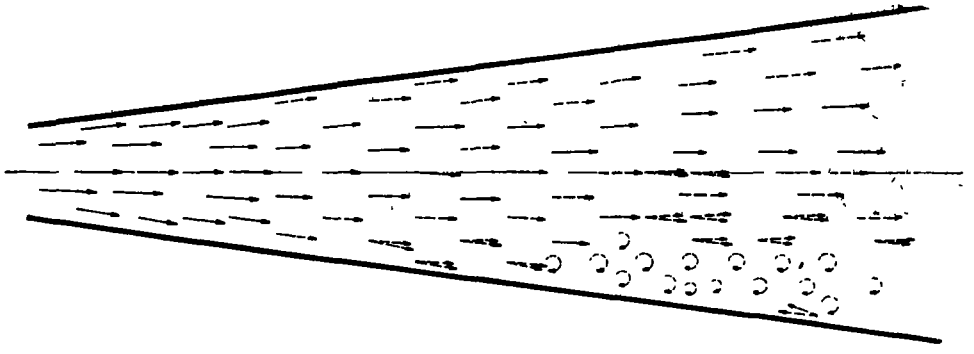

Figure 8. $\alpha = 16^{\circ}$.

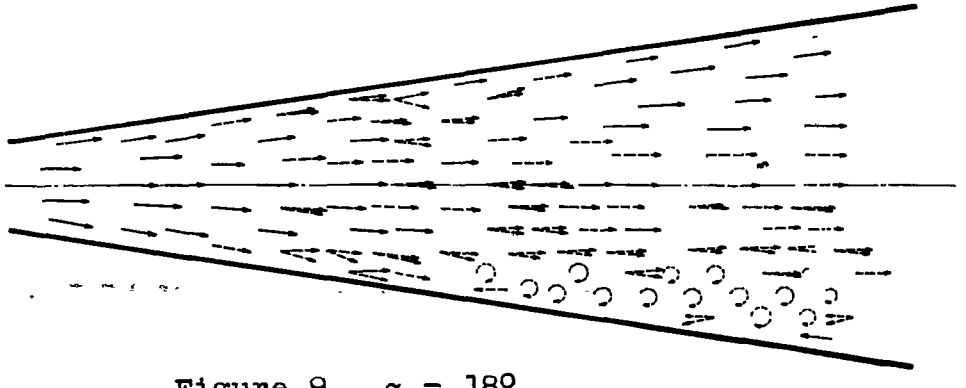

Figure 9. $\alpha = 18^{\circ}$.

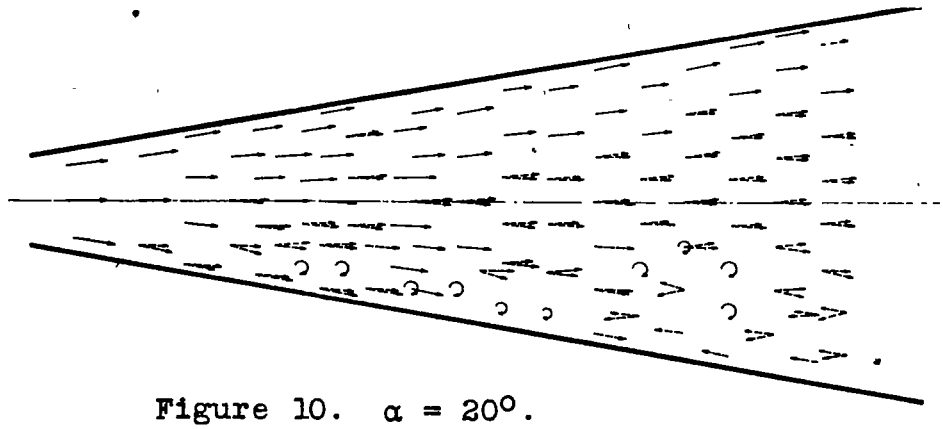

Figure 10. $\alpha = 20^{\circ}$.

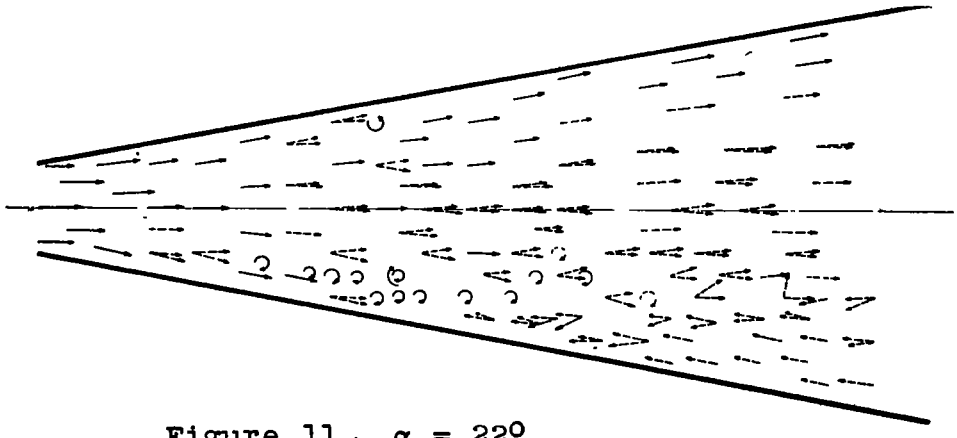

Figure 11. $\alpha = 22^{\circ}$.

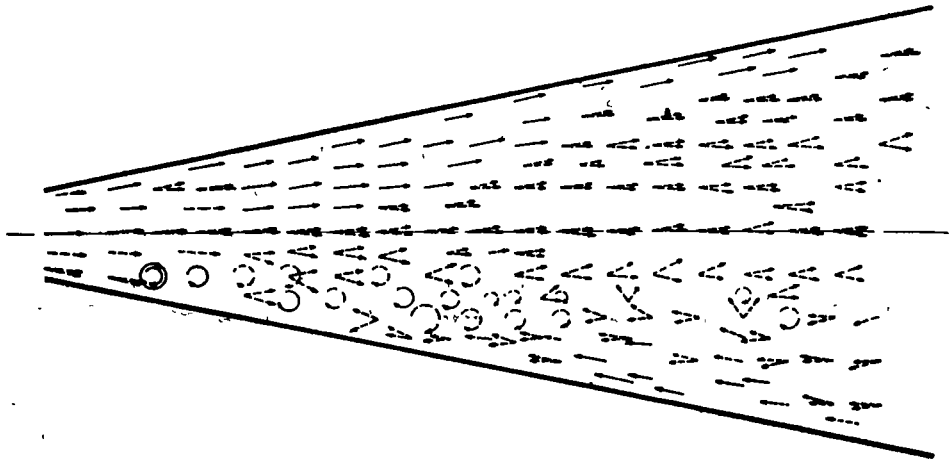

Figure 12. $\alpha = 24^{\circ}$.

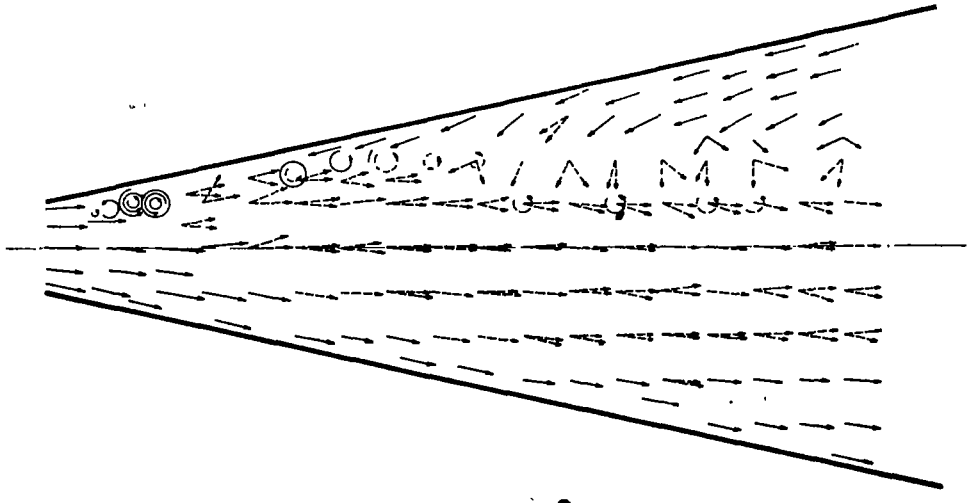

Figure 13. $\alpha = 26^{\circ}$.

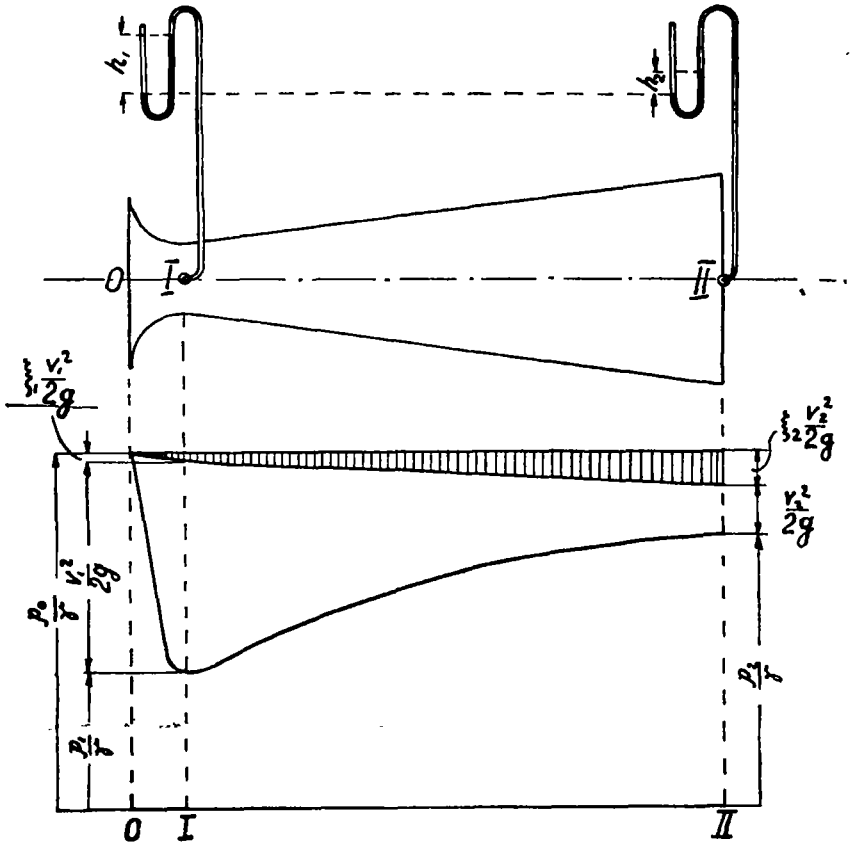

Figure 14.

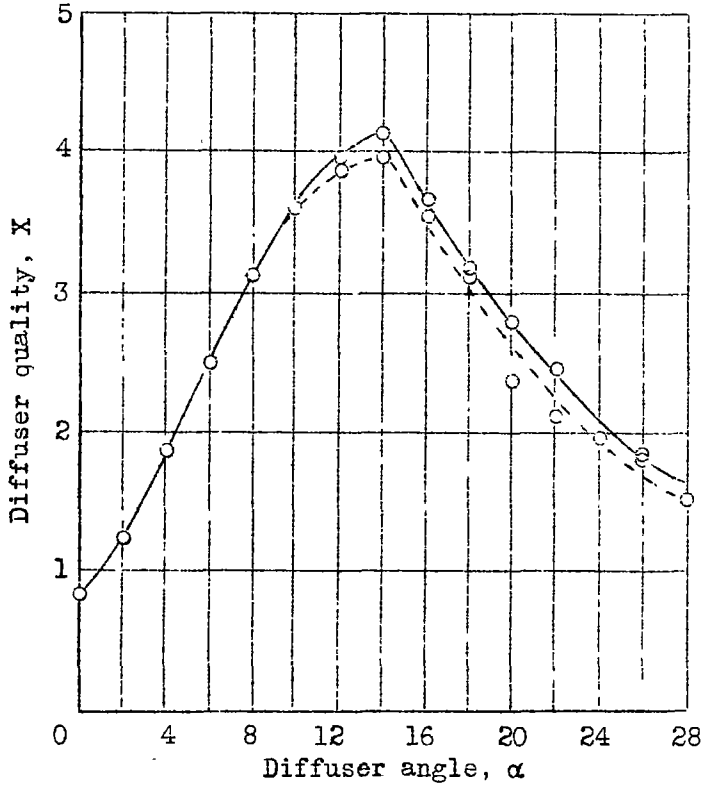

Fig. 15.

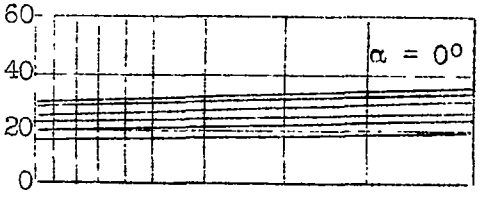

Fig. 16.

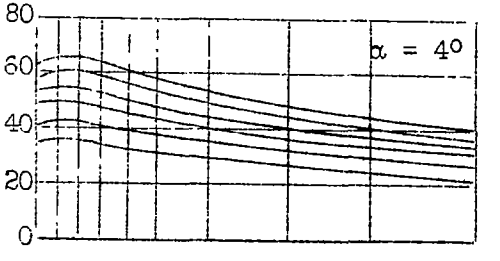

Fig. 17.

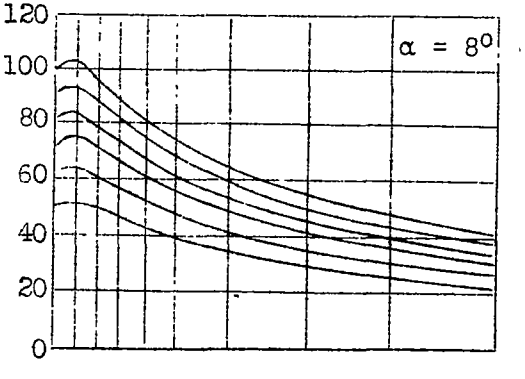

Fig. 18

Figures 16 to 18.- Negative static pressure distribution along diffuser axis for various velocities and diffuser angles.

Figure 19.

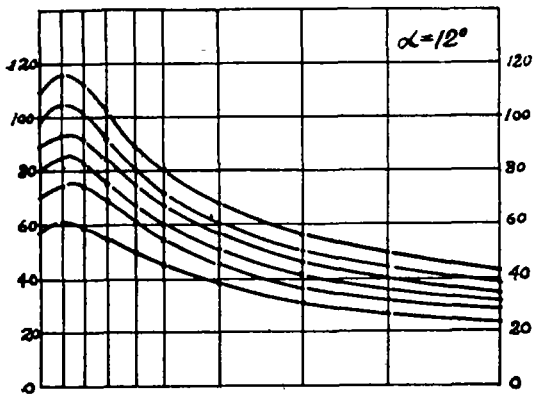

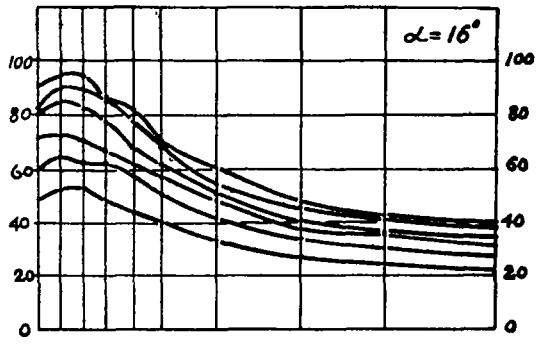

Figure 20.

Figures 19 to 22.- Negative static pressure distribution along diffuser axis for various velocities and diffuser angles.

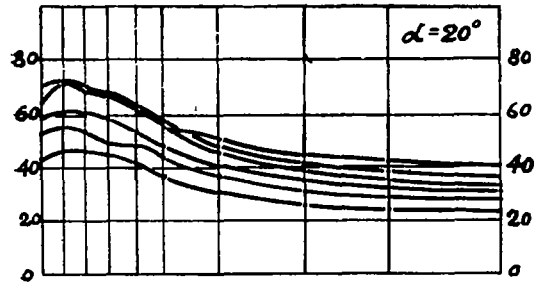

Figure 21.

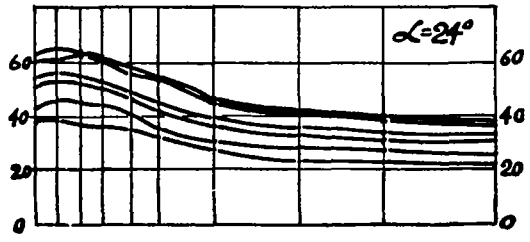

Figure 22.

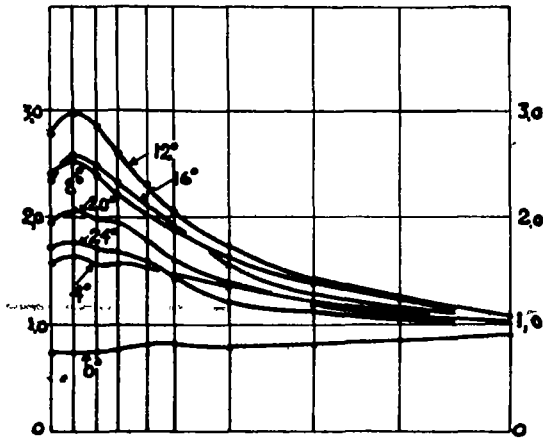

Fig. 23.- Ratio of mean pressure along diffuser axis to pressure in chamber.

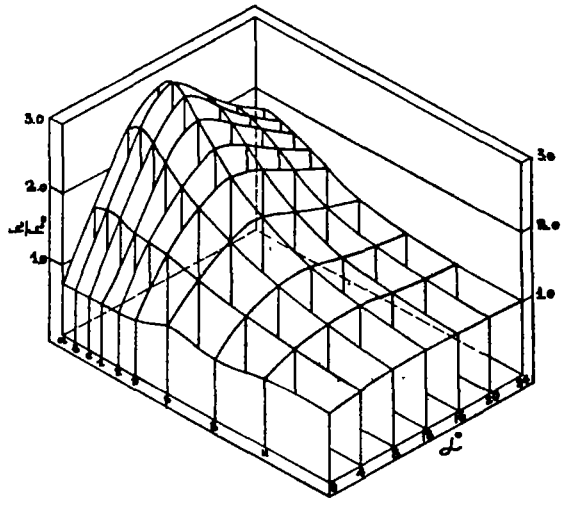

Fig. 24.- Pressure distribution in three dimensional representation.

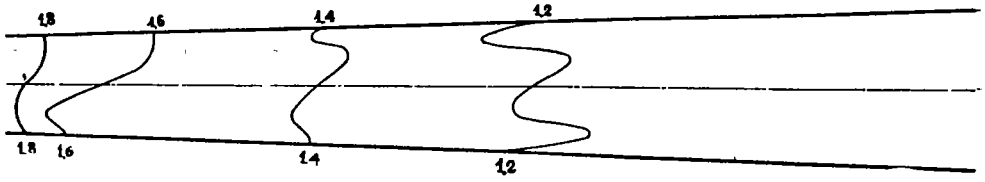

Figure 25. $\alpha = 4^{\circ}$.

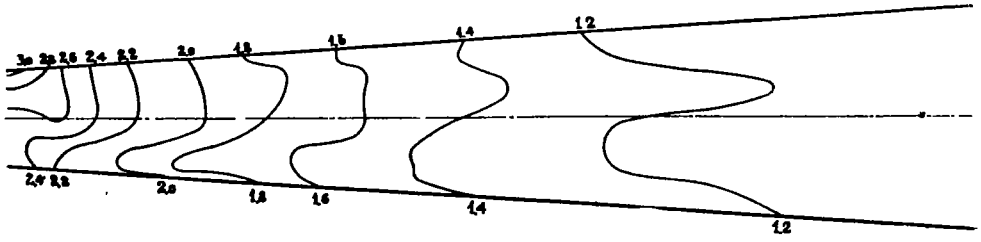

Figure 26. $\alpha = 8^{\circ}$.

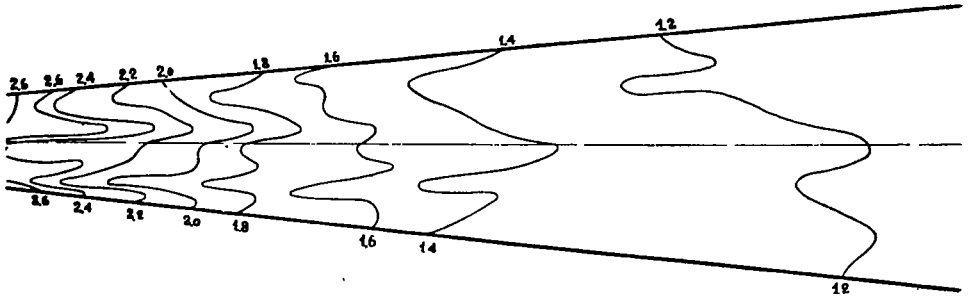

Figure 27. $\alpha = 12^{\circ}$.

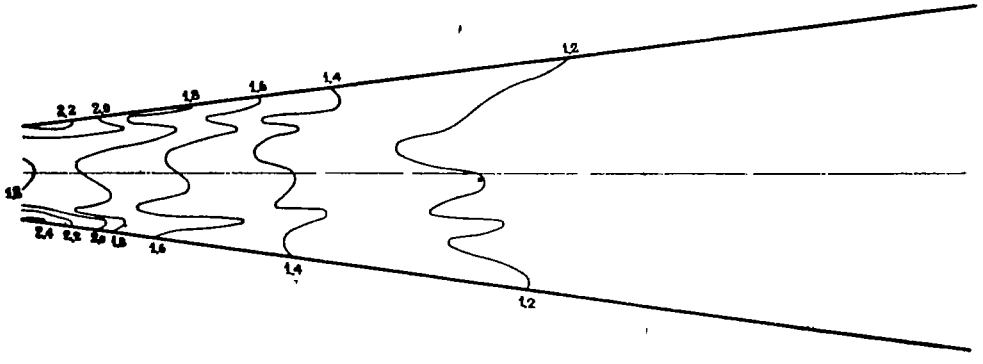

Figure 28. $\alpha = 16^{\circ}$.

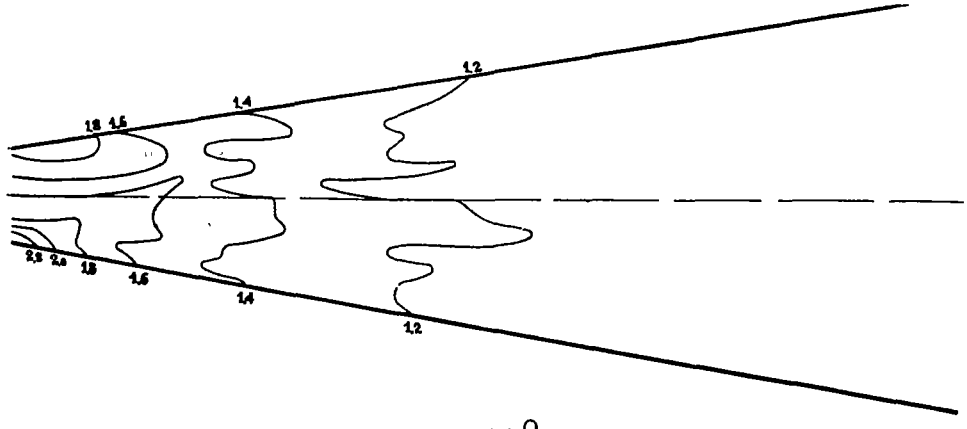

Figure 29. $\alpha = 20^{\circ}$.

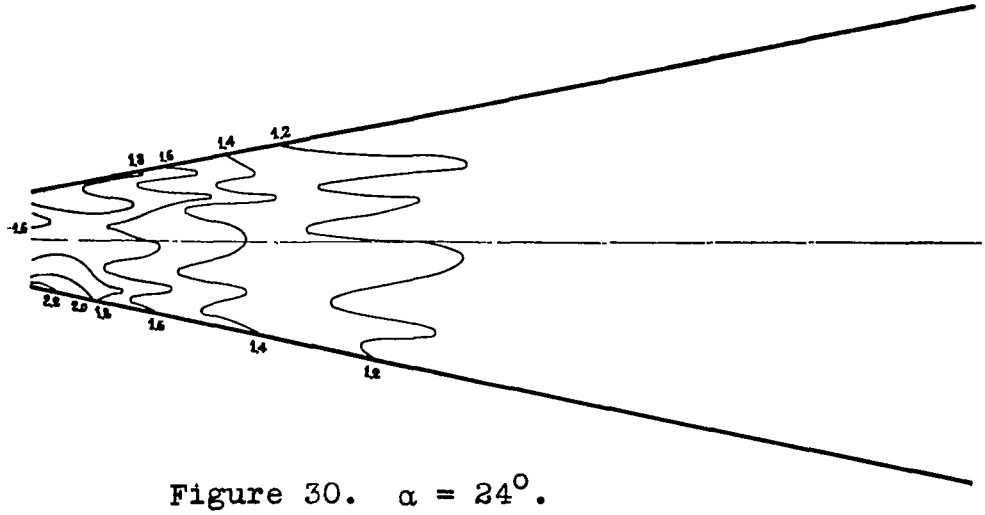

Figure 30. $\alpha = 24^{\circ}$.

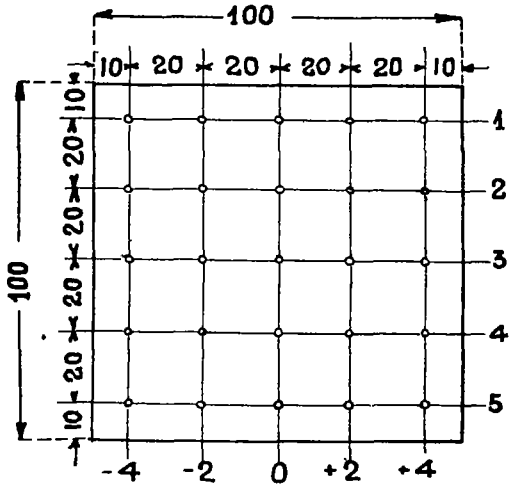

Figure 31.

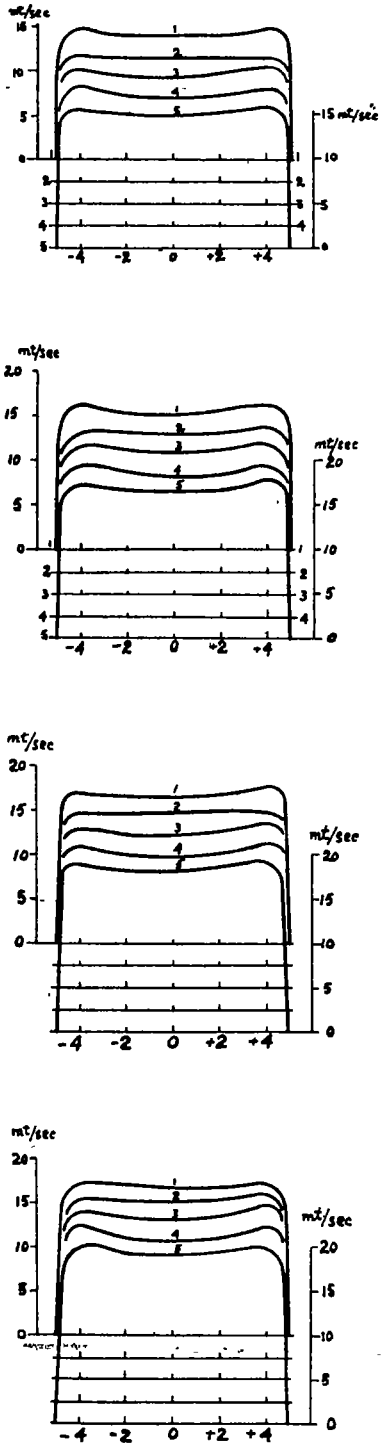

Figs. 32 to 35.- Velocity distribution for $\alpha = 0^{\circ}$.

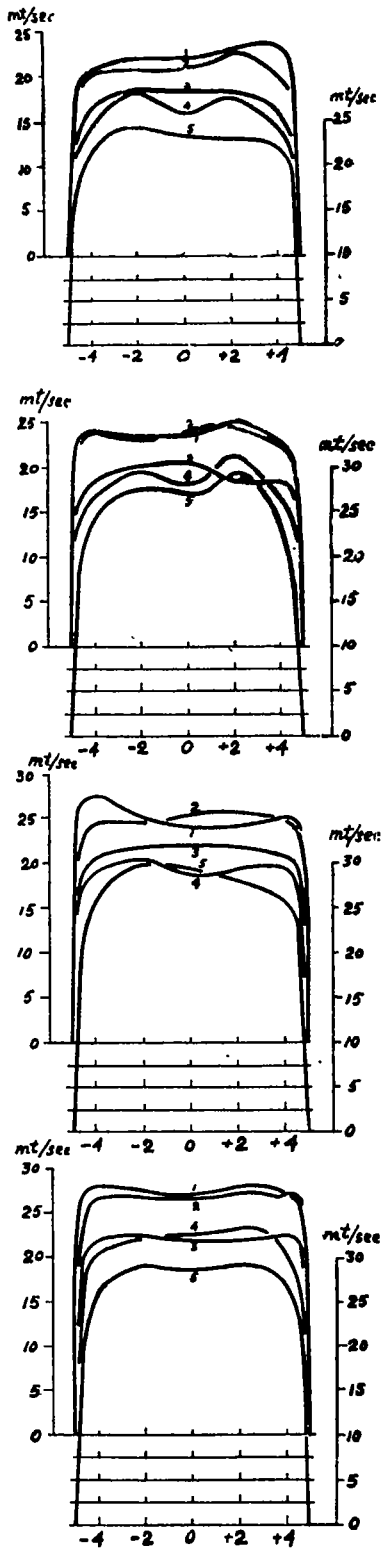

Figs. 36 to 39.- Velocity distribution in initial section for $\alpha = 24^{\circ}$.

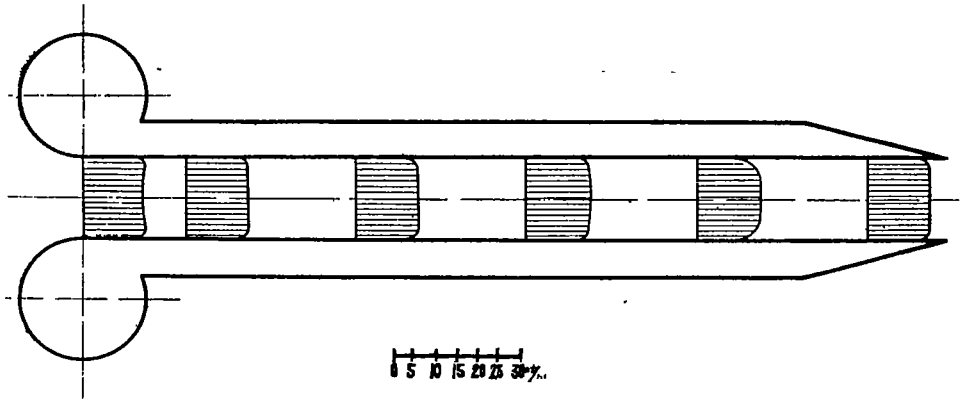

Figure 40. $\alpha = 0^{\circ}$

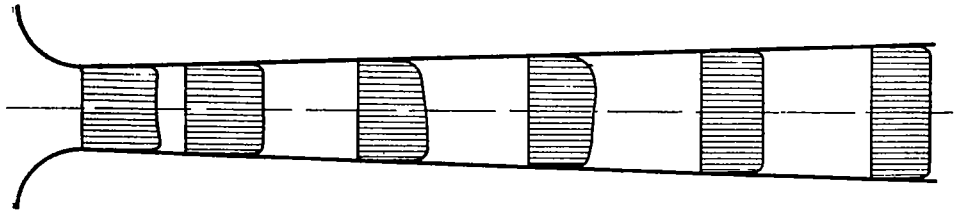

Figure 41. $\alpha = 4^{\circ}$.

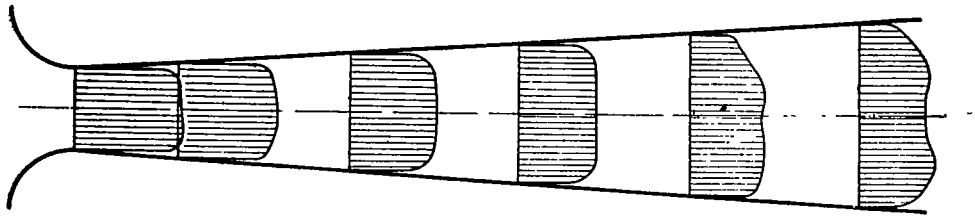

Figure 42. $\alpha = 8^{\circ}$.

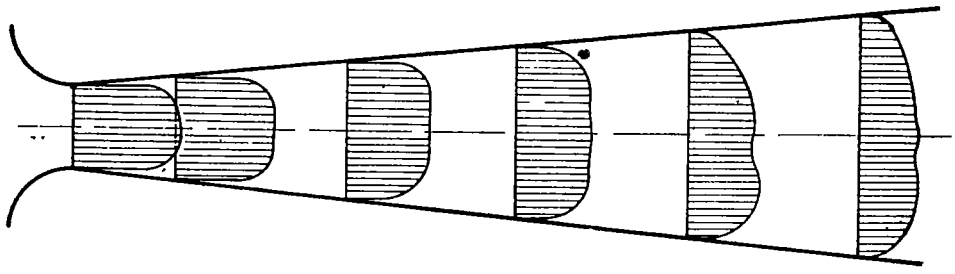

Figure 43. $\alpha = 12^{\circ}$.

Figs. 44,45,46,47

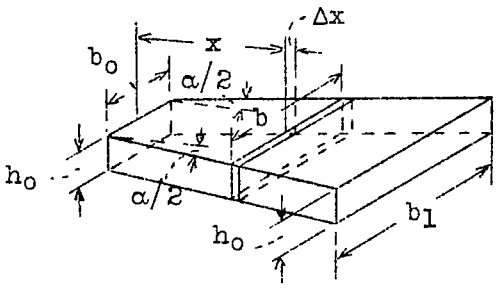

Fig. 44

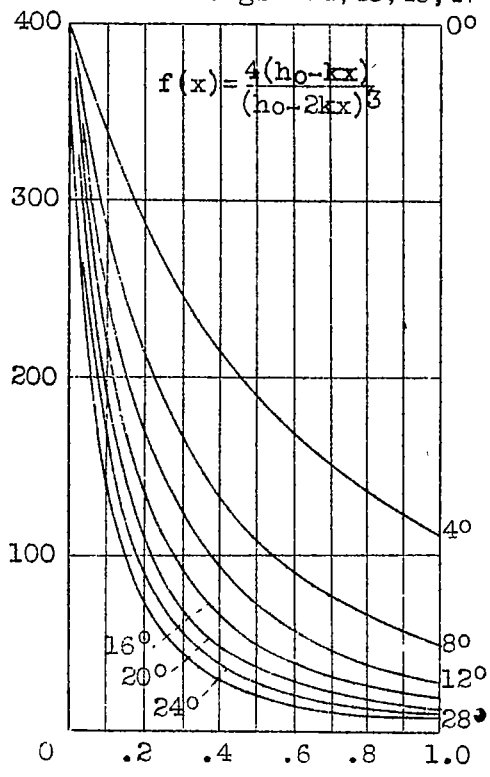

Fig. 45

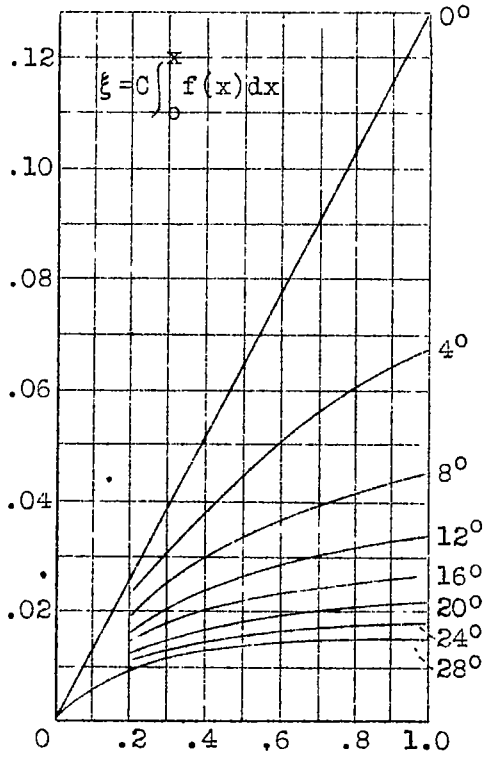

Fig. 46

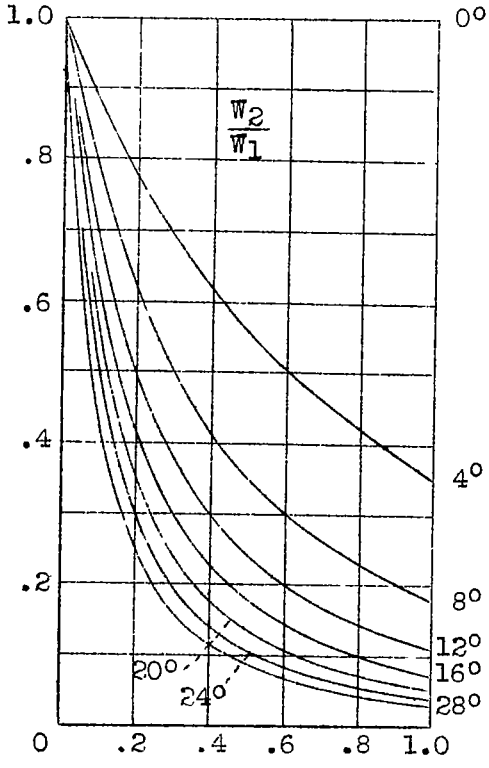

Fig. 47

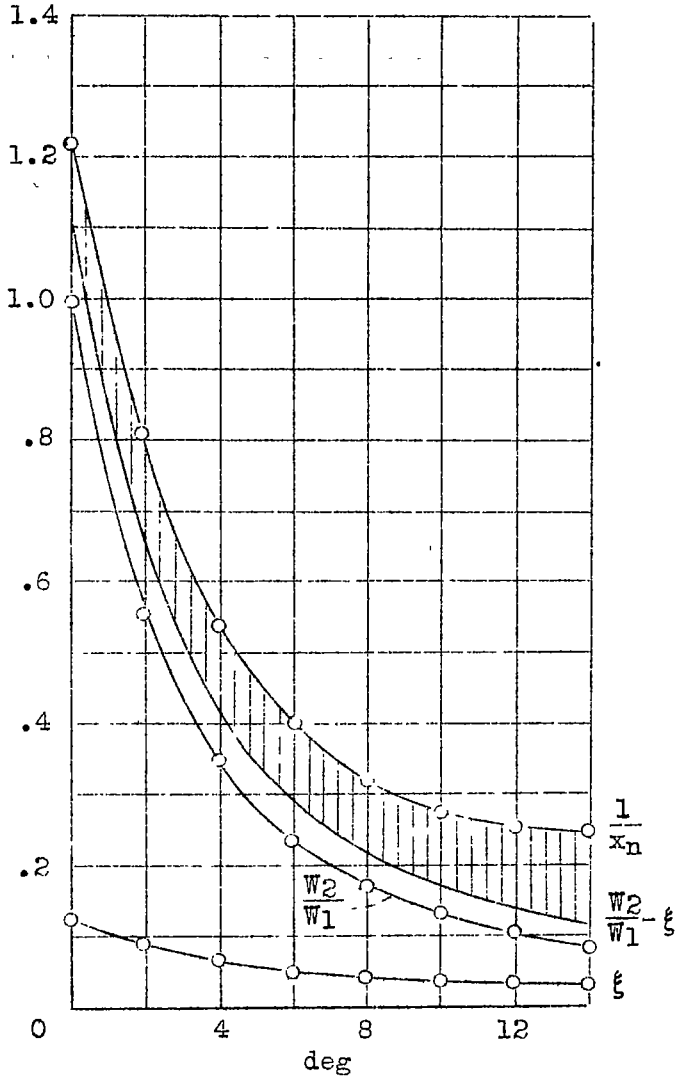
1.4
1.2
1.0
.8
.6
.4
.2
0
4
8
12
deg
$\frac{1}{x_n}$
$\frac{W_2}{W_1}$
$\frac{W_2}{W_1} - \xi$
ξ

Fig. 48.

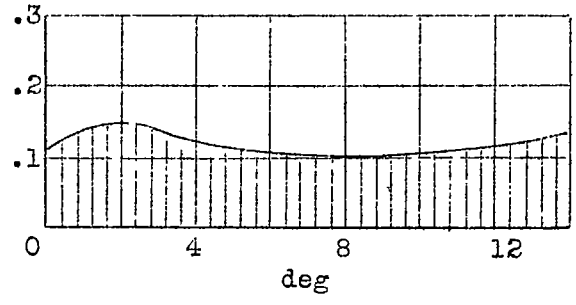
.3
.2
.1
0
4
8
12
deg

Fig. 49.